SIAM J. Appl. Math.
Vol. 75, No. 2, pp. 836–860

MATHEMATICAL MODELLING OF SURFACTANT SELF-ASSEMBLY AT INTERFACES*

C. E. MORGAN†, C. J. W. BREWARD†, I. M. GRIFFITHS‡, AND P. D. HOWELL†

Abstract. We present a mathematical model to describe the distribution of surfactant pairs in a multilayer structure beneath an adsorbed monolayer. A mesoscopic model comprising a set of ordinary differential equations that couple the rearrangement of surfactant within the multilayer to the surface adsorption kinetics is first derived. This model is then extended to the macroscopic scale by taking the continuum limit that exploits the typically large number of surfactant layers, which results in a novel third-order partial differential equation. The model is generalized to allow for the presence of two adsorbing boundaries, which results in an implicit free-boundary problem. The system predicts physically observed features in multilayer systems such as the initial formation of smaller lamellar structures and the typical number of layers that form in equilibrium.

Key words. adsorption kinetics, partial differential equations, free-boundary problems

AMS subject classifications. 35Q99, 35R37, 92A40, 92E99

DOI. 10.1137/140983641

1. Introduction.

Surfactant mixtures are used in a wide range of domestic and personal care products [11, 12]. The use of multiple surfactants in such products provides a synergistic enhancement in performance and flexibility in processing. Typically, mixed surfactant systems exhibit more pronounced interfacial adsorption than single surfactant systems [7]. Furthermore, the addition of an electrolyte to a mixed surfactant solution significantly may increase the concentration of surfactant adsorbed at the interface compared with the solution in the absence of electrolyte [9, 10, 14]. In such cases, surfactant is observed to adsorb not only as a monolayer at an interface but as a *multilayer* structure that extends into the bulk beneath the interface [9].

The accumulation of surfactant near an interface is a desirable property that is exploited in many applications. For example, in commercial and industrial detergents, a higher interfacial surfactant concentration improves the cleaning performance. Understanding the self-assembly process of multilayers at interfaces is vital in gaining insight into the mechanism by which detergent formulations work and in biological applications such as lipid multilayer formation in cell membranes [1]. In recent years, multilayer formation has been observed in porcine and bovine samples of pulmonary surfactant in vitro by Follows et al. [4]. Furthermore, exogenous surfactant is used therapeutically in the treatment of infant respiratory distress syndrome, a condition often suffered by premature neonates born before 26 weeks, gestation that arises due to a lack of type II pneumocytes, which secrete pulmonary surfactant in the lungs [6, 13]. Despite their numerous applications, the properties that govern the formation

*Received by the editors August 25, 2014; accepted for publication (in revised form) February 19, 2015; published electronically April 28, 2015. This work was partially supported by Award No. KUK-C1-013-04, made by King Abdullah University of Science and Technology (KAUST).
http://www.siam.org/journals/siap/75-2/98364.html
†Mathematical Institute, University of Oxford, Andrew Wiles Building, Radcliffe Observatory Quarter, Woodstock Road, Oxford, OX2 6GG, UK (morgan@maths.ox.ac.uk, breward@maths.ox.ac.uk, howell@maths.ox.ac.uk). The first author's work was supported by EPSRC via a CASE award.
‡Corresponding author. Mathematical Institute, University of Oxford, Andrew Wiles Building, Radcliffe Observatory Quarter, Woodstock Road, Oxford, OX2 6GG, UK (ian.griffiths@maths.ox.ac.uk).

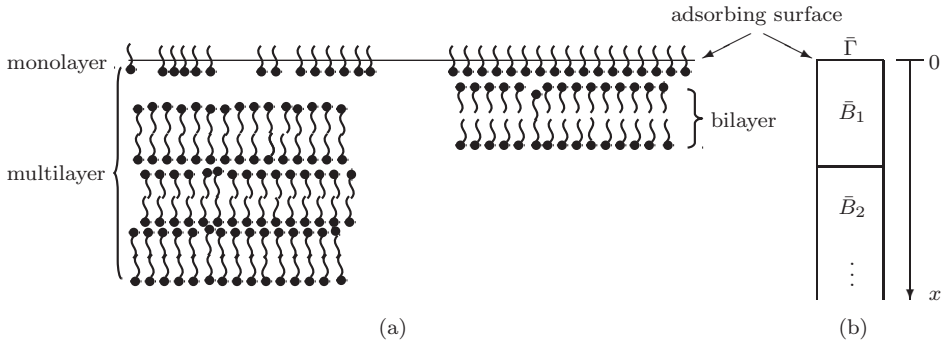

FIG. 1. *Schematic diagram of a surfactant multilayer structure and* (b) *the simplified model set-up.*

of such surfactant multilayers are yet to be fully characterized. In current applications of surfactant systems it is the dynamic and not the static properties that are of more importance, and a greater understanding would enable these properties to be optimized and the functionality of the system to be improved.

In this paper we present a mathematical model for the self-assembly of surfactant in a multilayer structure such as those observed in [9, 10, 14], neglecting the effect of any counterions that may be present and any bulk solution effects such as aggregation. We consider two situations: (i) the adsorption of a surfactant multilayer at an interface and (ii) the adsorption of a surfactant solution onto two surfaces that are in close proximity to one another. For the first situation we consider the mesoscopic problem and derive a semidiscrete model to describe the movement of surfactant between each layer in the multilayer structure. We then extend this model to the macroscopic scale and derive a one-dimensional, third-order, nonlinear partial differential equation to describe the spatiotemporal evolution of a multilayer structure. For the second situation we show that the macroscopic model is described by an implicit free-boundary problem.

2. Modeling assumptions. We consider the formation of a surfactant multilayer structure beneath a monolayer adsorbed at a surface that may be either solid or liquid. The multilayer structure consists of a series of stacked bilayers and each bilayer is a planar arrangement of surfactant monomer pairs that are adsorbed either to a monomer at the surface or to a monomer pair in an adjacent bilayer (Figure 1(a)). When in such an adsorbed configuration, we refer to these monomer pairs as *surfactant pairs* or *bilayer molecules*, as opposed to dimers, which we use to refer to pairs of surfactant molecules bound together in the bulk solution.

In this paper we are concerned only with the behavior of the surfactant in the multilayer structure and so neglect any free monomer or aggregates in the bulk that are typically present in such systems [9, 10, 14]. Thus, in our model surfactant can exist only either as surfactant pairs in a bilayer or as adsorbed monomer in the monolayer.

We neglect any electrostatic effects that may be present between bilayers and model the movement of bilayer molecules between adjacent layers as an adsorption process. We consider a one-dimensional domain $\mathcal{D} := \{x : x \in [0, \infty]\}$, where the x-axis points downward into the solution and the boundary $x = 0$ corresponds to the adsorbing surface. The domain $\mathcal{D}$ is divided into K compartments each of length h so that the ith compartment represents the ith bilayer in the multilayer structure, and we denote the total number of bilayer molecules in this compartment by $\bar{B}_i$. We assume

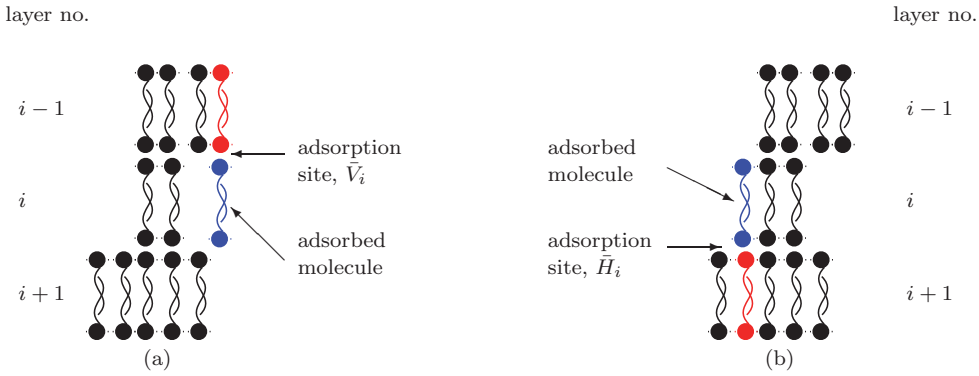

FIG. 2. *Schematic diagram for the two possible adsorption sites available for a molecule existing in the ith compartment:* (a) $\bar{V}_i = (\bar{B}_{i-1} - \bar{B}_i)^+$; (b) $\bar{H}_i = (\bar{B}_{i+1} - \bar{B}_i)^+$.

that surfactant bilayer molecules must dissociate into monomers before adsorbing at the surface $x = 0$ and we denote the number of adsorbed surfactant monomers at the interface of our set-up by $\bar{\Gamma}$. A schematic of the simplified model set-up we consider is shown in Figure 1(b).

We assume that bilayer molecules can only move to adjacent compartments, i.e., to a compartment directly above (closer to the interface) or below (further from the interface), and only do so provided there is an available adsorption site. An adsorption site is simply a space in a bilayer where a bilayer molecule in the layer above or below has not been covered. Specifically, a molecule may move into the ith layer by adsorbing onto an exposed molecule that is in either the $(i-1)$th or $(i+1)$th compartment, as shown in Figure 2. We denote the number of available adsorption sites in the $(i-1)$th layer onto which a molecule in the ith layer may adsorb by[1]

$$\bar{V}_i = (\bar{B}_{i-1} - \bar{B}_i)^+. \tag{2.1}$$

The number of available adsorption sites in the $(i+1)$th layer to which a molecule in the ith layer may adsorb is denoted by

$$\bar{H}_i = (\bar{B}_{i+1} - \bar{B}_i)^+. \tag{2.2}$$

The possible adsorption sites are shown schematically in Figure 2.

Assuming that the movement of bilayer molecules between adjacent layers is spontaneous we may write down a series of single-step "reactions" for their movements. The movement of a molecule in the $(i+1)$th compartment to the ith compartment can be written in reaction form as follows:

$$\mathcal{B}_{i+1} + \mathcal{V}_i \xrightarrow{\bar{a}_i} \mathcal{B}_i \quad \text{for} \quad i = 1, \ldots, K, \tag{2.3a}$$

$$\mathcal{B}_{i+1} + \mathcal{H}_i \xrightarrow{\bar{c}_i} \mathcal{B}_i \quad \text{for} \quad i = 2, \ldots, K, \tag{2.3b}$$

[1]Throughout this paper we use the notation $(\cdot)^+$, which is defined by $(z)^+ = \frac{1}{2}(z + |z|) = \begin{cases} z, & z \geq 0, \\ 0, & z < 0. \end{cases}$

where $\mathcal{B}_i, \mathcal{H}_i, \mathcal{V}_i$ denote the species in the ith compartment (i.e., either a bilayer molecule or a vacancy), and $\bar{a}_i$ and $\bar{c}_i$ denote the corresponding rate constants for the reactions. Here, the total number of vacancies in the first bilayer is given by

$$\bar{V}_1 = \bar{\Gamma} - \bar{B}_1. \tag{2.4}$$

Similarly, the movement of a molecule in the $(i-1)$th compartment to the ith compartment can be written in reaction form as

$$\mathcal{B}_{i-1} + \mathcal{V}_i \overset{\bar{b}_i}{\to} \mathcal{B}_i \quad \text{for} \quad i = 2, \ldots, K, \tag{2.5a}$$

$$\mathcal{B}_{i-1} + \mathcal{H}_i \overset{\bar{d}_i}{\to} \mathcal{B}_i \quad \text{for} \quad i = 2, \ldots, K, \tag{2.5b}$$

and $\bar{b}_i$ and $\bar{d}_i$ denote the corresponding rate constants for the reactions.

At the adsorbing surface a bilayer molecule in the first bilayer may dissociate into two monomers, which then adsorb to the surface provided it is not saturated. If the monolayer is not saturated, that is, $\bar{\Gamma} < \bar{\Gamma}_{\text{sat}}$, say, then the number of vacant adsorption sites is given by

$$\bar{V}_{\text{m}} = \bar{\Gamma}_{\text{sat}} - \bar{\Gamma}, \tag{2.6}$$

where the subscript "m" notation is used to denote the different species in the monolayer.

Similarly, two adsorbed monomers from the monolayer may spontaneously desorb and form a bilayer molecule in the first bilayer provided there is an available adsorption site. The number of available adsorption sites for molecules in the first bilayer is given by

$$\bar{V}_1 = (\bar{\Gamma} - \bar{B}_1)^+ \quad \text{and} \quad \bar{H}_1 = (\bar{B}_2 - \bar{B}_1)^+. \tag{2.7}$$

We assume that the adsorption-desorption processes associated with the monolayer occur as single-step reactions given by

$$\mathcal{B}_1 + 2\mathcal{V}_{\text{m}} \overset{\bar{a}_{\text{m}}}{\to} 2\mathcal{G}, \qquad 2\mathcal{G} + \mathcal{V}_1 \overset{\bar{b}_{\text{m}}}{\to} \mathcal{B}_1, \qquad 2\mathcal{G} + \mathcal{H}_1 \overset{\bar{d}_{\text{m}}}{\to} \mathcal{B}_1, \tag{2.8}$$

where $\mathcal{G}$ denotes an adsorbed monomer in the monolayer, $\mathcal{V}_{\text{m}}$ denotes a vacancy in the monolayer, and $\bar{a}_{\text{m}}, \bar{b}_{\text{m}}$, and $\bar{d}_{\text{m}}$ are the corresponding rate constants.

3. Mesoscopic model.

3.1. Governing equations. The areal concentration of adsorbed monomers in the monolayer ($\text{mol}\,\text{m}^{-2}$) at time $\hat{t}$ is given by $\hat{\Gamma}(\hat{t}) = N_A\bar{\Gamma}(\hat{t})/A$, where N_A is Avogadro's constant and A is the interfacial surface area of our domain. Similarly, the concentration of bilayer molecules in the ith bilayer ($\text{mol}\,\text{m}^{-2}$) at time $\hat{t}$ is given by $\hat{B}_i(\hat{t}) = N_A\bar{B}_i(\hat{t})/A$ for $i = 1, \ldots, K$. We nondimensionalize the model by rescaling the variables as follows:

$$\hat{t} = \frac{K^3}{\bar{a}_1\Gamma_{\text{sat}}h^3}t, \qquad \hat{\Gamma} = \Gamma_{\text{sat}}\Gamma, \qquad \hat{B}_i = \Gamma_{\text{sat}}B_i \quad \text{for} \quad 1 \le i \le K, \tag{3.1}$$

where Γ_{sat} is the saturation concentration of the monolayer ($\text{mol}\,\text{m}^{-2}$) and h is the depth of a bilayer molecule. The timescale is chosen to conserve a dominant balance when we consider the continuum approximation in section 4. We invoke the law of

mass action to obtain a system of $(K+1)$ ordinary differential equations (ODEs) for $\Gamma, B_1, \ldots, B_K$:

$$\epsilon^3 \frac{\mathrm{d}\Gamma}{\mathrm{d}t} = 2\left(Q^a_{\mathrm{m}} - Q^b_{\mathrm{m}} - Q^d_{\mathrm{m}}\right), \tag{3.2a}$$

$$\epsilon^3 \frac{\mathrm{d}B_1}{\mathrm{d}t} = -\left(Q^a_{\mathrm{m}} - Q^b_{\mathrm{m}} - Q^d_{\mathrm{m}}\right) + Q^a_1 - Q^b_2 + Q^c_1 - Q^d_2, \tag{3.2b}$$

$$\epsilon^3 \frac{\mathrm{d}B_i}{\mathrm{d}t} = Q^a_i - Q^a_{i-1} + Q^b_i - Q^b_{i+1} + Q^c_i - Q^c_{i-1} + Q^d_i - Q^d_{i+1}$$

$$\text{for} \quad i = 2, \ldots, K-2, \tag{3.2c}$$

$$\epsilon^3 \frac{\mathrm{d}B_{K-1}}{\mathrm{d}t} = Q^a_{K-1} - Q^a_{K-2} + Q^b_{K-1} - Q^b_K + Q^c_{K-1} - Q^c_{K-2} + Q^d_{K-1}, \tag{3.2d}$$

$$\epsilon^3 \frac{\mathrm{d}B_K}{\mathrm{d}t} = -Q^a_{K-1} + Q^b_K - Q^c_{K-1}, \tag{3.2e}$$

where $\epsilon = 1/K$, and the fluxes are given by

$$Q^a_{\mathrm{m}} = a_{\mathrm{m}} V^2_{\mathrm{m}} B_1 = a_{\mathrm{m}}(1-\Gamma)^2 B_1, \tag{3.3a}$$

$$Q^b_{\mathrm{m}} = b_{\mathrm{m}} V_1 \Gamma^2 = b_{\mathrm{m}} \left(\Gamma - B_1\right)^+ \Gamma^2, \tag{3.3b}$$

$$Q^d_{\mathrm{m}} = d_{\mathrm{m}} H_1 \Gamma^2 = d_{\mathrm{m}} (B_2 - B_1)^+ \Gamma^2, \tag{3.3c}$$

$$Q^a_1 = V_1 B_2 = (\Gamma - B_1)^+ B_2, \tag{3.3d}$$

$$Q^a_i = a_i V_i B_{i+1} = a_i (B_{i-1} - B_i)^+ B_{i+1} \qquad \text{for} \quad i = 2, \ldots, K-1, \tag{3.3e}$$

$$Q^b_i = b_i V_i B_{i-1} = b_i (B_{i-1} - B_i)^+ B_{i-1} \qquad \text{for} \quad i = 2, \ldots, K, \tag{3.3f}$$

$$Q^c_i = c_i H_i B_{i+1} = c_i (B_{i+1} - B_i)^+ B_{i+1} \qquad \text{for} \quad i = 1, \ldots, K-1, \tag{3.3g}$$

$$Q^d_i = d_i H_i B_{i-1} = d_i (B_{i+1} - B_i)^+ B_{i-1} \qquad \text{for} \quad i = 2, \ldots, K-1. \tag{3.3h}$$

Here $a_{\mathrm{m}}, b_{\mathrm{m}}$, and d_{m} are the dimensionless rate constants for the surface reactions, scaled with $\bar{a}_1/\Gamma_{\mathrm{sat}}$, and a_i, b_i, c_i, and d_i are the dimensionless bulk rate constants, scaled with $\bar{a}_1$, so $a_1 = 1$; V_i and H_i correspond to the dimensionless concentration of vacancies above and beneath the ith bilayer, respectively, scaled with Γ_{sat}, and V_{m} corresponds to the dimensionless concentration of vacancies in the monolayer, scaled with Γ_{sat}. To close the system we prescribe the initial conditions

$$\Gamma(0) = \Gamma_0 \quad \text{and} \quad B_i(0) = B_{i_0} \quad \text{for} \quad i = 1, \ldots, K \tag{3.4}$$

for some constants Γ_0 and B_{i_0} for $i = 1, \ldots, K$.

Upon summation of (3.2a)–(3.2e) and integration with respect to t we obtain an equation expressing mass conservation,

$$\Gamma(t) + 2\sum_{i=1}^{K} B_i(t) = \Gamma_0 + 2\sum_{i=1}^{K} B_{i_0} := \mathcal{S}, \tag{3.5}$$

where $\mathcal{S}$ is a constant and denotes the total dimensionless concentration of surfactant in the system.

3.2. Steady-state solutions. We first examine the steady-state solutions of (3.2). To simplify the analysis we make the assumption that $B_i \leq B_{i-1}\ \forall\ 1 \leq i \leq K$. This is physically reasonable since we anticipate a decreasing concentration of surfactant with depth, and indeed this has been observed in such systems as those described in [9]. We note that there exists no empirical method to measure all the rate parameters in the model, and so to proceed further we assume that the constants a_i and b_i are equal, i.e., $a_i = b_i = c_i = d_i = 1$ for $i = 1, \ldots, K$ (since the rate constants have been scaled with $\bar{a}_1$). Since we do not expect a molecule existing in the ith layer to experience any directional preference in the site into which it adsorbs, this assumption is physically reasonable. However, we may expect the adsorption behavior at the interface to differ from within the bulk, so we make no assumptions on the size of a_{m} and b_{m}. The steady-state configuration is determined by setting

$$Q^a_{\mathrm{m}} - Q^b_{\mathrm{m}} - Q^d_{\mathrm{m}} = Q^a_i - Q^b_{i+1} = Q^c_i = Q^d_i = 0 \quad \forall \quad 1 \leq i \leq K, \tag{3.6}$$

which yields

$$B_i = \Gamma \left(\frac{\Gamma^2}{\Gamma^2 + a^*(1-\Gamma)^2} \right)^i \quad \text{for} \quad i = 1, \ldots, K. \tag{3.7}$$

Here $a^* = a_{\mathrm{m}}/b_{\mathrm{m}}$ is the ratio of adsorption to desorption rates, i.e., if $a^* > 1$, then the equilibrium between the monolayer and the first bilayer shifts to favor existence in the adsorbed monolayer state, while if $a^* < 1$, then the equilibrium favors existence in the bilayer.

Given the concentration of surfactant in the monolayer, Γ, (3.7) provides the concentration of surfactant in the subsequent bilayers. The monolayer concentration may be determined via conservation of mass (3.5), which provides the implicit relationship

$$\begin{aligned} \mathcal{S} &= \Gamma \left(1 + 2 \sum_{i=1}^{K} \left(\frac{\Gamma^2}{\Gamma^2 + a^*(1-\Gamma)^2} \right)^i \right) \\ &= \Gamma \left(1 + \frac{2\Gamma^2}{a^*(1-\Gamma)^2} \left[1 - \left(\frac{\Gamma^2}{\Gamma^2 + a^*(1-\Gamma)^2} \right)^K \right] \right). \end{aligned} \tag{3.8}$$

In the limit $K \to \infty$ and when Γ is not close to 1, (3.8) simplifies to give a cubic equation for Γ:

$$a^*(\Gamma - \mathcal{S})(1-\Gamma)^2 + 2\Gamma^3 = 0. \tag{3.9}$$

For all positive values of a^* and $\mathcal{S}$, there is a unique real solution of (3.9) for $\Gamma \in (0,1)$, the behavior of which as a function of $\mathcal{S}$ resembles a Langmuir-type isotherm [2] between the bulk and surface concentrations (see Figure 3(a)). Furthermore, we note that (3.9) reduces to

$$\Gamma \sim \mathcal{S} - 2\frac{\mathcal{S}^3}{a^*} + \cdots \qquad \text{as} \quad \mathcal{S} \to 0. \tag{3.10}$$

In the case when $K \to \infty$ and $\Gamma \sim 1$, the asymptotic expansion of (3.8) yields

$$\Gamma \sim 1 - \sqrt{\frac{2\xi}{a^*\mathcal{S}}}, \tag{3.11}$$

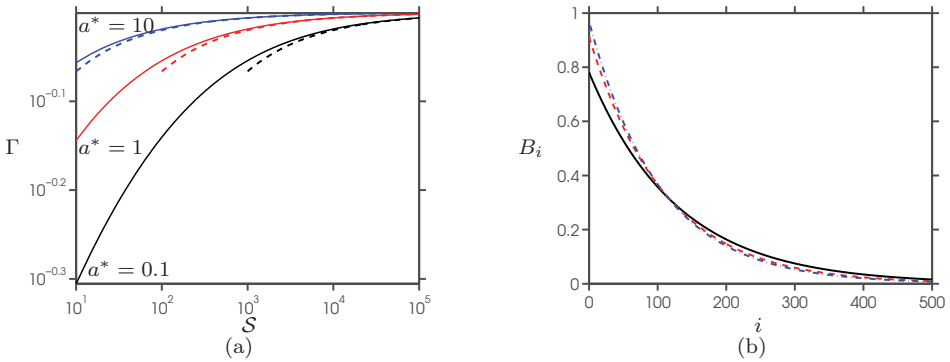

FIG. 3. (a) *Steady-state surface concentration* Γ*, given by* (3.9) *(continuous lines) and the leading-order asymptotic approximation* (3.10) *(dashed lines) versus total surfactant concentration,* $\mathcal{S}$*.* (b) *The steady-state distribution of surfactant in the multilayer structure,* B_i*, given by* (3.7) *for* $\mathcal{S} = 200$*, with* $a^* = 0.1$ *(black continuous line),* 1 *(red dashed line), and* 10 *(blue dot-dashed line).*

where ξ is given by solving

$$-\frac{\log(1-\xi)}{\xi} = \frac{2K}{\mathcal{S}} \equiv \frac{1}{M}, \tag{3.12}$$

and M is a measure of the surfactant per unit layer. In the limit when $K \to \infty$ and $K/\mathcal{S} \to \infty$, $\xi \to 1$ and (3.11) reduces to the asymptotic expansion given by taking the limit $\mathcal{S} \to \infty$ in (3.9).

For the physical scenarios of interest in this paper, the net concentration of surfactant is large compared with the concentration of surfactant in each cell, so henceforth we shall consider the case $\mathcal{S} \gg 1$. The asymptotic approximation in this limit, (3.10), provides an excellent representation of the dependence of the surface concentration on total surfactant concentration, as shown in Figure 3(a). Using this expression for Γ the resulting steady-state distribution of surfactant within the multilayer is given by (3.7) and is presented in Figure 3(b).

3.2.1. Time-dependent solutions. In this section we compute the solutions to the system of ODEs (3.2) using the MATLAB solver `ode45` for the parameters $K = 100$, $a_\mathrm{m} = 2$, $b_\mathrm{m} = d_\mathrm{m} = 0.2$, and $a_i = b_i = c_i = d_i = 1$ for $i = 1, \ldots, K$. Three scenarios for the initial distribution of bilayers are of interest:

1. Physically, one expects the distribution to be monotonically decreasing with depth [9] so it is reasonable to assume that the initial conditions are given by a monotonically decreasing distribution. Thus, we solve the system of ODEs (3.2) subject to the initial conditions
(3.13)
$$\Gamma_0 = 0.8, \quad B_{i_0} = \Gamma_0 \exp\left(-\left(\frac{i}{\sigma(K+1)}\right)^2\right) \quad \text{for} \quad 1 \le i \le K, \quad \sigma = 0.3.$$
The surfactant concentration is observed to transition smoothly from the initial configuration to the steady-state solution (3.7) as t increases (Figure 4(a)). During the evolution, each bilayer undergoes a transient period in which the concentration fluctuates as the multilayer structure reorganizes among the layers (Figure 4(b), (c)). Following this, the concentration of adsorbed surfactant at the interface rises above its equilibrium value, before approaching this from above (Figure 4(d)).

2. We next consider the situation where the initial concentration of each bilayer is randomly distributed over $[0, 1]$, simulating a randomly arranged surfactant structure in solution, whose concentrations are shown for the example considered here by the red crosses in Figure 5(a). As Figures 5(a) and (b) show, there is a rapid transient from the noisy initial data to a seemingly smooth distribution by time $t \approx 10^{-3}$, following which the concentration in each bilayer converges to the steady-state distribution on an order-one timescale. We also observe an interesting feature of the formation of "smooth humps" and "sharp troughs" for small time in Figure 5(a), which indicate that the system evolves to the final multilayer structure by first forming smaller multilayer regions (separated by the sharp troughs of much lower concentration), which eventually combine to form the full multilayer structure. It has indeed been observed experimentally that during the formation of a full multilayer in linear alkylbenzene surfactants the structure is often first fragmented into lamellae, in a disordered "mosaic spread" [8]. The fact that the model is able to reproduce such features that are characteristic of the transition that the multilayer structure evolves through is encouraging.
3. Finally, we consider a set-up in which the surfactant is uniformly distributed in each bilayer but the concentration in the adsorbing surface is zero. Such a configuration could describe a scenario in which the surfactant solution is placed in a container with a lid, which is instantaneously removed at $t = 0$. In this case, Figure 6 shows that, after an initial transient, the distribution of bilayer molecules evolves in an almost identical way to that with the randomly distributed initial condition shown in Figure 5, with the formation of smaller regions of higher concentration (smooth peaks) again separated by regions of lower concentration (sharp troughs).

Motivated by the apparent piecewise continuous behavior of the concentration distribution displayed in Figures 4–6, which arises as a result of the typically large number of bilayers in a multilayer structure, in the following section we make a continuum approximation to the system of ODEs (3.2) to derive a partial differential equation (PDE) that describes a macroscopic model for the system evolution.

4. Macroscopic model.

4.1. Governing equation. We now consider the limit $\epsilon = 1/K \to 0$ to derive a continuum approximation to the system of ODEs (3.2). Then, $B(x, t)$ provides the continuous approximation to the concentration of bilayer molecules in the ith compartment where

$$B(x, t) \approx B_i(t), \quad x = i\epsilon. \tag{4.1}$$

Similarly we define

$$Q_a(x, t) \approx Q_i^a(t), \quad Q_b(x, t) \approx Q_i^b(t), \quad Q_c(x, t) \approx Q_i^c(t), \quad Q_d(x, t) \approx Q_i^d(t), \tag{4.2}$$

and, assuming these are all smooth, continuously differentiable functions of x and t, we expand (3.2c) as a Taylor series about $\epsilon = 0$. This leads to

$$\epsilon^3 \frac{\partial B}{\partial t} = \epsilon \frac{\partial}{\partial x}\left(Q_a - Q_b + Q_c - Q_d\right) - \frac{1}{2}\epsilon^2 \frac{\partial^2}{\partial x^2}\left(Q_a - Q_b + Q_c - Q_d\right) + O(\epsilon^3), \tag{4.3}$$

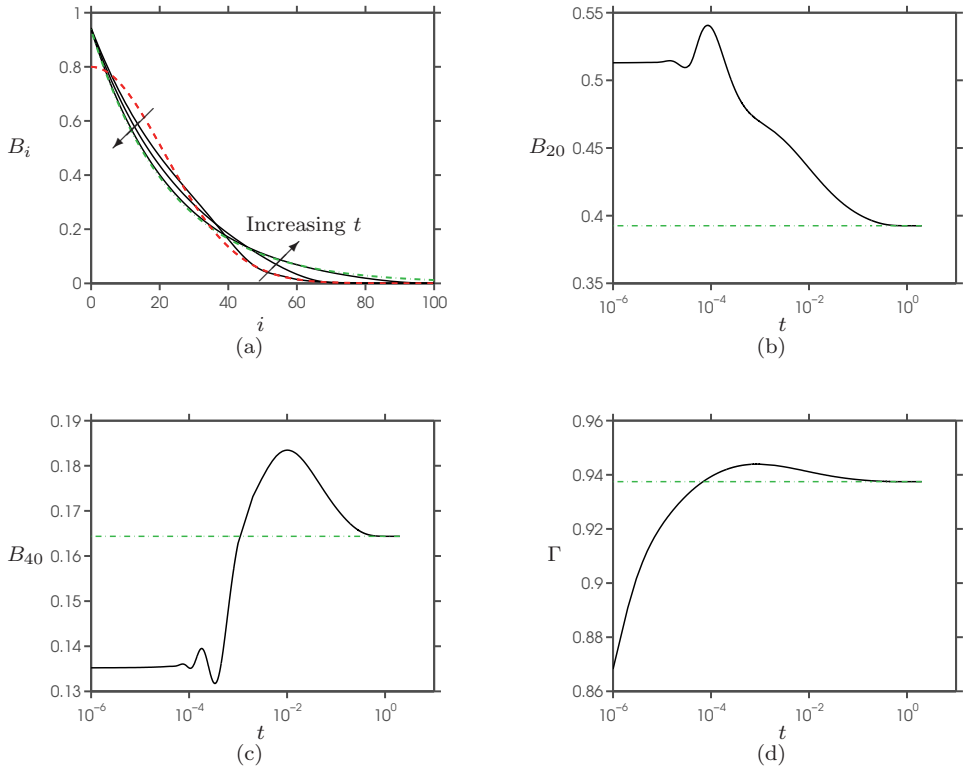

FIG. 4. *Plots of the numerical solutions to the system of ODEs* (3.2) *subject to the initial conditions* (3.13). (a) *The numerical solution to* B_i *(solid black lines) versus* i *at times* $t = 0.001, 0.01, 0.1$. *The initial condition* (3.13) *and steady-state solution* (3.7) *are shown as the red dashed line and green dot-dashed line, respectively.* (b)–(d) *Comparison of the numerical solutions (black line) with the steady-state solutions* (3.7) *(green, dot-dashed line) for* B_{20}, B_{40}, *and* Γ. *Here* $a_m = 2$, $b_m = d_m = 0.2$, $a_i = b_i = c_i = d_i = 1$ *for* $i = 1, \ldots, K$ *and* $K = 100$.

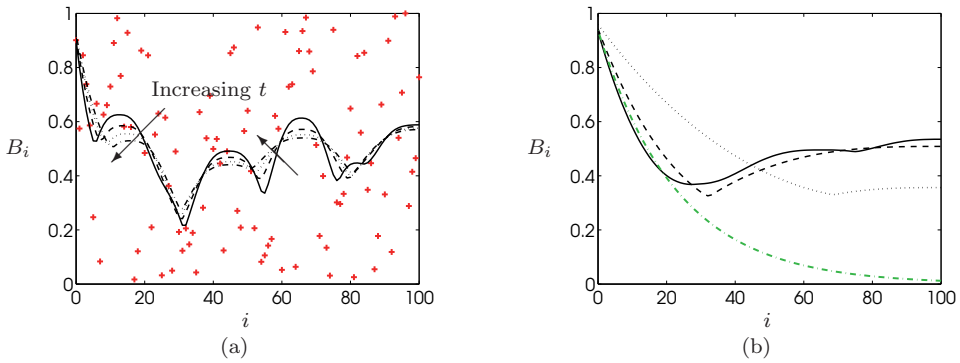

FIG. 5. *Plots of the numerical solutions to the system of ODEs* (3.2) *for* (a) *random initial data (red crosses) and at times* $t = 5 \times 10^{-5}$ *(black solid line),* $t = 1 \times 10^{-4}$ *(black dashed line),* $t = 1.5 \times 10^{-4}$ *(black dotted line), and* $t = 2 \times 10^{-4}$ *(black dot-dashed line);* (b) *times* $t = 1 \times 10^{-3}$ *(black solid line),* $t = 1 \times 10^{-2}$ *(black dashed line),* $t = 1 \times 10^{-1}$ *(black dotted line) and the green dot-dashed curve denotes the steady-state solution* (3.7). *Here* $a_m = 2$, $b_m = d_m = 0.2$, $a_i = b_i = c_i = d_i = 1$ *for* $i = 1, \ldots, K$ *and* $K = 100$.

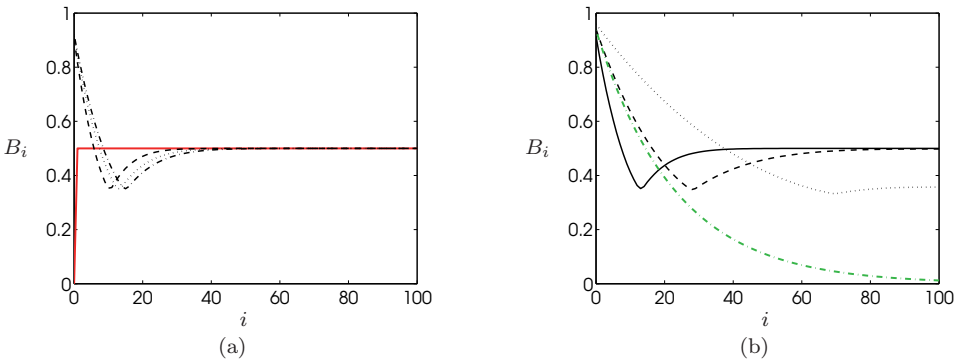

FIG. 6. *Plots of the numerical solutions to the system of ODEs* (3.2) *(black lines) for* (a) *uniform initial data (red continuous line) and for the time intervals* $t \in [5 \times 10^{-4}, 10^{-3}, 1 \times 10^{-3}]$*;* (b) *times* $t = 1 \times 10^{-3}$ *(black solid line),* $t = 1 \times 10^{-2}$ *(black dashed line),* $t = 1 \times 10^{-1}$ *(black dotted line), and the green dot-dashed curve denotes the steady-state solution* (3.7)*. Here* $a_m = 2$*,* $b_m = d_m = 0.2$*,* $a_i = b_i = c_i = d_i = 1$ *for* $i = 1, \ldots, K$ *where* $K = 100$*.*

where

$$Q_a(x,t) = a(x)\theta[-B_x]\left(-\epsilon B B_x - \epsilon^2 {B_x}^2 + \frac{\epsilon^2}{2} B B_{xx}\right) + O(\epsilon^3), \tag{4.4a}$$

$$Q_b(x,t) = b(x)\theta[-B_x]\left(-\epsilon B B_x + \epsilon^2 {B_x}^2 + \frac{\epsilon^2}{2} B B_{xx}\right) + O(\epsilon^3), \tag{4.4b}$$

$$Q_c(x,t) = c(x)\theta[B_x]\left(\epsilon B B_x + \epsilon^2 {B_x}^2 + \frac{\epsilon^2}{2} B B_{xx}\right) + O(\epsilon^3), \tag{4.4c}$$

$$Q_d(x,t) = d(x)\theta[B_x]\left(\epsilon B B_x - \epsilon^2 {B_x}^2 + \frac{\epsilon^2}{2} B B_{xx}\right) + O(\epsilon^3), \tag{4.4d}$$

and $\theta[\cdot]$ is the Heaviside function.

As assumed thus far, on the microscopic scale, a bilayer molecule should express no bias toward which direction it will move nor to which adsorption site it will occupy. Thus, we set the coefficients $a(x) = b(x) = c(x) = d(x) = 1$. Under this assumption, at leading order, (4.3) reduces to the third-order nonlinear PDE

$$\frac{\partial B}{\partial t} = \frac{\partial}{\partial x}\left(\mathrm{sgn}(B_x)\left({B_x}^2 - B B_{xx}\right)\right), \qquad 0 < x < \infty, \quad 0 < t. \tag{4.5}$$

4.2. Boundary conditions. We expect to impose three boundary conditions on the third-order PDE (4.5), which we derive from the continuum approximation to the ODEs at either end of the discretized domain $\mathcal{D}$. First we consider the boundary condition at the adsorbing surface, $x = 0$, by expanding the dimensionless versions of (3.2a), (3.2b), and (3.2c) for $i = 2$ about $\epsilon = 0$. This gives

$$\frac{\epsilon^3}{2}\dot{\Gamma} = J_{\mathrm{m}} \qquad \text{at} \quad x = 0, \tag{4.6a}$$

$$\epsilon^3 B_t + \epsilon^4 B_{tx} + \cdots = J_1 - J_{\mathrm{m}} \qquad \text{at} \quad x = 0, \tag{4.6b}$$

$$\epsilon^3 B_t + 2\epsilon^4 B_{tx} + \cdots = J_2 - J_1 \qquad \text{at} \quad x = 0, \tag{4.6c}$$

where $\dot{}$ denotes differentiation with respect to t and

$$J_{\rm m} = Q^a_{\rm m} - Q^b_{\rm m} - Q^d_{\rm m}, \tag{4.7a}$$

$$J_1 = Q^a_1 - Q^b_2 + Q^c_1 - Q^d_2, \tag{4.7b}$$

$$J_2 = Q^a_2 - Q^b_3 + Q^c_2 - Q^d_3. \tag{4.7c}$$

Summing (4.6a)–(4.6c) leads to

$$\frac{\epsilon^3}{2}\dot{\Gamma} + 2\epsilon^3 B_t + 3\epsilon^4\epsilon B_{tx} + \cdots = J_2 \quad \text{at} \quad x = 0. \tag{4.8}$$

With $a(x) = b(x) = c(x) = d(x) = 1$, (4.8) implies that

$$B_x^2 - BB_{xx} = 0 \quad \text{on} \quad x = 0, \tag{4.9}$$

to leading order, while (4.6b) at leading order gives

$$0 = \theta[\Gamma - B](\Gamma - B)B \quad \text{on} \quad x = 0. \tag{4.10}$$

Assuming that $a_{\rm m}, b_{\rm m}$, and $d_{\rm m}$ are $O(1)$ as $\epsilon \to 0$, (4.6a) gives, to leading order,

$$0 = a_{\rm m}(1-\Gamma)^2 B - b_{\rm m}\theta[\Gamma - B]\Gamma^2(\Gamma - B) \quad \text{on} \quad x = 0. \tag{4.11}$$

Provided $B(0,t) \neq 0$, (4.10) implies that either $\Gamma = B(0,t)$ or $\Gamma < B(0,t)$. If the latter were true, then (4.11) would imply that $B(0,t) > 1$, which contradicts the modeling assumption that there is a unit dimensionless saturation concentration in the monolayer and bilayers. Thus, by (4.11) the final boundary condition at the adsorbing surface is

$$\Gamma = B = 1 \quad \text{on} \quad x = 0. \tag{4.12}$$

This condition indicates that the monolayer equilibrates much more rapidly than the multilayer (the dynamics could be captured asymptotically by considering a shorter timescale). It is, however, possible to obtain a distinguished limit in which the monolayer evolves on the same timescale as the multilayer structure if $a_{\rm m}$, $b_{\rm m}$, and $d_{\rm m}$ are order ϵ^3. In this case, on setting $a_{\rm m} = \epsilon^3\alpha_{\rm m}$, $b_{\rm m} = \epsilon^3\beta_{\rm m}$, and $d_{\rm m} = \epsilon^3\delta_{\rm m}$, the leading-order terms in (4.6)–(4.8) provide the boundary conditions

$$B_x^2 - BB_{xx} = 0 \quad \text{on} \quad x = 0, \tag{4.13a}$$

$$\text{with} \quad B(0,t) = \Gamma(t) \quad \text{and} \quad \frac{{\rm d}\Gamma}{{\rm d}t} = 2\alpha_{\rm m}(1-\Gamma)^2\Gamma. \tag{4.13b}$$

Equation (4.13b) represents the kinetic adsorption of surfactant monomers from the first bilayer onto the adsorbing surface and possesses similar characteristics to the well-known Langmuir–Hinshelwood equation for adsorption of free surfactant monomers from the bulk [2].

Equation (4.13b) can be integrated with respect to t to obtain an implicit expression for $\Gamma(t)$, namely,

$$\log\left(\frac{\Gamma}{1-\Gamma}\right) + \frac{1}{1-\Gamma} = 2\alpha_{\rm m}t + \log\left(\frac{\Gamma_0}{1-\Gamma_0}\right) + \frac{1}{1-\Gamma_0}, \tag{4.14}$$

where $\Gamma(0) = \Gamma_0 < 1$. We note that the limiting behavior of $\Gamma(t)$ in (4.14) for $t \ll 1$ and as $t \to \infty$ is given by

$$\Gamma \sim \Gamma_0 \left(1 + 2\alpha_{\mathrm{m}}(1-\Gamma_0)^2 t + \cdots\right) \qquad \text{as} \quad t \to 0, \tag{4.15a}$$

$$\Gamma \sim 1 - \frac{1}{2\alpha_{\mathrm{m}} t} + \cdots \qquad \text{as} \quad t \to \infty. \tag{4.15b}$$

Thus, the adsorbed concentration will increase linearly for early time and approach the dimensionless (unit) saturation concentration algebraically for large times.

Next we consider the boundary condition at the bottom of the multilayer by expanding the sum of (3.2d) and (3.2e), which yields

$$3\epsilon^3 B_t - 3\epsilon^4 B_{tx} + \cdots = J_{K-1} \quad \text{at} \quad x = 1, \tag{4.16}$$

where $J_{K-1} = -Q^a_{K-2} + Q^b_{K-1} - Q^c_{K-2} + Q^d_{K-1}$. Again we set $a(x) = b(x) = c(x) = d(x) = 1$ to obtain, at leading order,

$$B_x^2 - BB_{xx} = 0 \quad \text{at} \quad x = 1. \tag{4.17}$$

Integrating (4.5) with respect to x and applying the boundary conditions (4.9) and (4.17) yields an expression for net conservation of surfactant,

$$\frac{\mathrm{d}}{\mathrm{d}t}\left(\int_0^1 B(x,t)\,\mathrm{d}x\right) = 0. \tag{4.18}$$

Equation (4.18) is consistent with (3.5) which gives, as $\epsilon \to 0$,

$$M = \int_0^1 B(x,t)\,\mathrm{d}x, \tag{4.19}$$

where $M = \epsilon\mathcal{S}/2$ is the normalized net concentration of bilayers as introduced in (3.12) and is assumed to be order one. Note that $M \le 1$, with $M = 1$ corresponding to all layers being completely filled.

4.3. Steady-state solution. Considering the steady version of (4.5) subject to the boundary conditions (4.9) and (4.17) we find that the steady-state concentration profile satisfies

$$(B')^2 - BB'' = 0, \quad \text{where} \quad {}' := \frac{\mathrm{d}}{\mathrm{d}x}, \tag{4.20}$$

which can be integrated subject to the boundary condition (4.12) (or (4.13b)) to give the general solution

$$B(x) = \mathrm{e}^{-kx}. \tag{4.21}$$

The net concentration condition (4.19) implies that

$$M = \frac{1}{k}\left(1 - \mathrm{e}^{-k}\right). \tag{4.22}$$

As discussed in section 3.2, for the physical scenarios of interest we expect the concentration of bilayers in the multilayer to decrease with depth, and so we expect that $k > 0$. The parameter k provides an estimate of the number of bilayers that we

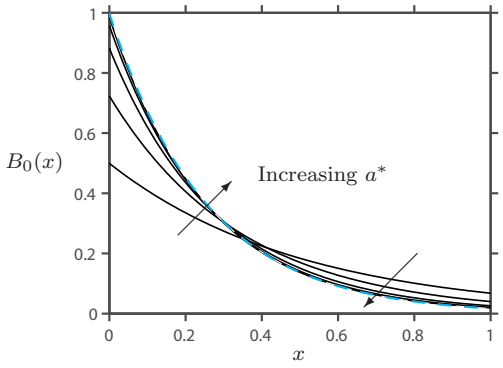

FIG. 7. *Comparison of the steady-state solution* (4.21) *of the macroscopic model (blue curve) with the steady-state solution* (3.7) *and* (3.9) *of the mesoscopic model for* $a^* = 10^{-1}, 10, 10^1$, *and* 10^2 *(black curves), with* $K = 200$ *and* $\mathcal{S} = 100$.

would expect to form for a given concentration of surfactant, M, with preliminary experiments suggesting qualitative agreement with the predicted result (4.22) [8].

We note that although this continuum model predicts that the equilibrium surface concentration, Γ, is equal to unity (from (4.12)), the mesoscopic model predicts that the adsorbed concentration is not necessarily equal to unity (equation (3.8)). However, as shown in (3.10), the steady-state value of Γ approaches 1 asymptotically as $\mathcal{S} \to \infty$, which is a requirement of the continuum model to ensure a nonzero bulk surfactant concentration $M = \epsilon\mathcal{S}/2$ in the limit $\epsilon \to 0$, and so this result is asymptotically consistent. As observed in Figure 7, the steady-state solutions for the continuum model (4.21) compare well with the mesoscopic model, (3.7), and (3.9) when the parameter a^* is order one, with the difference between the two steady states $B(x)$ and B_i within the expected error $\epsilon = 1/K$. This discrepancy is reduced when $a^* \gg 1$ and increases when $a^* \ll 1$, which is to be expected from the asymptotic expansion of Γ as $\mathcal{S} \to \infty$ given in (3.10) for which this expansion is no longer valid.

4.4. Linear stability analysis. We consider a small perturbation to the steady-state solution (4.21) to determine if the perturbation decays with time and thus whether the steady-state solution we have found is linearly stable. Provided $B_x < 0$ for $x \in [0, 1]$ we perturb as follows:

$$B(x,t) = \mathrm{e}^{-kx} + \delta b(x,t), \quad \delta \ll 1; \tag{4.23}$$

upon substitution into (4.5) and linearizing with respect to δ we find that

$$b_t = -\mathrm{e}^{-kx}\left(k^3 b + k^2 b_x - k b_{xx} - b_{xxx}\right). \tag{4.24}$$

Seeking a separable solution to (4.24), $b(x,t) = X(\xi)\mathrm{e}^{\lambda k^3 t}$, where $\xi = kx$, we find that $X(\xi)$ and the normalized growth rate λ satisfy the eigenvalue problem

$$X(1 + \lambda \mathrm{e}^{\xi}) + X' - X'' - X''' = 0, \qquad 0 < \xi < k, \tag{4.25a}$$

$$X = X'' + 2X' = 0 \qquad \text{on} \quad \xi = 0, \tag{4.25b}$$

$$X'' + 2X' + X = 0 \qquad \text{on} \quad \xi = k. \tag{4.25c}$$

The amplitude of the eigenfunction $X(\xi)$ is arbitrary so we eliminate this degree of freedom by setting $X'(0) = 1$. We introduce the new dependent variables

$$u = \mathrm{e}^{\xi} X, \qquad v = \mathrm{e}^{\xi}(X' + X), \qquad w = \mathrm{e}^{-\xi}(X'' + 2X' + X) \tag{4.26}$$

to allow (4.25) to be written as the first-order system

$$u' = v, \quad v' = \mathrm{e}^{2\xi} w, \quad w' = \lambda \mathrm{e}^{-\xi} u, \tag{4.27}$$

subject to the boundary conditions

$$u = 0, \quad v = 1, \quad w = 0, \qquad \xi = 0, \tag{4.28a}$$

$$w = 0, \qquad \xi = k. \tag{4.28b}$$

If $\lambda > 0$, then (4.27) and (4.28a) imply that u, v, and w are all positive for $\xi > 0$ and hence condition (4.28b) cannot be satisfied. Thus $\lambda < 0$ and the steady-state solution is linearly stable. The eigenvalues may be determined numerically by solving the initial-value problem given by (4.27) and (4.28a) for a given (negative) value of λ and inferring the corresponding value of k that satisfies (4.28b).

For each domain length, k, there is a countably infinite set of negative eigenvalues, λ. As k decreases we observe that $|\lambda|$ rapidly increases and so for small values of $|\lambda|$, k must be large. This suggests that the solution to (4.25) may be approximated using the WKBJ method, by setting $X(\xi) \sim A(\xi)\mathrm{e}^{\phi(\xi)}$, which is valid when either $|\lambda|$ or k is large. The general solution given this ansatz is approximately given by

$$\begin{aligned} X(\xi) \sim \mathrm{e}^{-2\xi/3} \Bigg\{ & C_1 \mathrm{e}^{3\lambda^{1/3}\mathrm{e}^{\xi/3}} + C_2 \mathrm{e}^{-3\lambda^{1/3}\mathrm{e}^{\xi/3}/2} \cos\left(\frac{3\sqrt{3}\lambda^{1/3}\mathrm{e}^{\xi/3}}{2}\right) \\ & + C_3 \mathrm{e}^{-3\lambda^{1/3}\mathrm{e}^{\xi/3}/2} \sin\left(\frac{3\sqrt{3}\lambda^{1/3}\mathrm{e}^{\xi/3}}{2}\right) \Bigg\}, \end{aligned} \tag{4.29}$$

where C_1, C_2, and C_3 are integration constants. The boundary conditions (4.25b), (4.25c) lead to the solvability condition

$$\begin{aligned} & \frac{\sqrt{3}}{2} \sin\left(\frac{3\sqrt{3}\lambda^{1/3}}{2}\left(\mathrm{e}^{k/3} - 1\right)\right) + \frac{1}{2}\cos\left(\frac{3\sqrt{3}\lambda^{1/3}}{2}\left(\mathrm{e}^{k/3} - 1\right)\right) \\ & \qquad = \frac{1}{2}\exp\left(\frac{9\lambda^{1/3}}{2}\left(\mathrm{e}^{k/3} - 1\right)\right), \end{aligned} \tag{4.30}$$

whose solution, λ, may be written in the form

$$\lambda = -\left(\frac{2\left(\phi + \pi/6\right)}{3\sqrt{3}\left(\mathrm{e}^{k/3} - 1\right)}\right)^3, \tag{4.31}$$

where ϕ satisfies the transcendental equation

$$\sin\phi = -\frac{1}{2}\mathrm{e}^{-\sqrt{3}(\phi + \pi/6)}. \tag{4.32}$$

The solutions of (4.32) are approximately given by $\phi \approx n\pi$, where $n = 1, 2, 3, \ldots$, and hence the eigenvalues are given approximately by

$$\lambda \sim -\left(\frac{(6n+1)\pi}{9\sqrt{3}\left(\mathrm{e}^{k/3} - 1\right)}\right)^3, \qquad n = 1, 2, 3, \ldots. \tag{4.33}$$

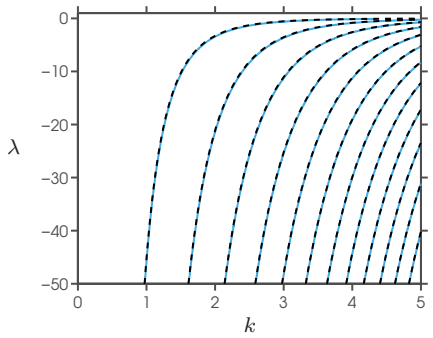

FIG. 8. *Linear growth rate λ versus domain size k for the eigenvalue problem* (4.25). *The solid blue curves are found by numerical solution of* (4.27)*; the black dashed curves show the approximation given by* (4.33).

The approximation (4.33) provides an excellent representation of the numerically determined eigenvalues from the full system, (4.27), as observed in Figure 8.

We note that for the problem on the semi-infinite domain, the steady-state solution (4.21) is exponentially small for large x and one cannot linearize (4.5) about an exponentially small function in x. Thus, the problem is nonuniform in the limit $k \to \infty$, which corresponds to the semi-infinite domain. In this limit the eigenvalues, λ, in (4.33) are all exponentially small and the corresponding eigenfunctions, X, have unbounded amplitude.

4.5. Time-dependent solutions. Given smooth initial data $B(x,0) = B_0(x)$ the PDE (4.5), boundary conditions (4.9), (4.17), and (4.12) (or (4.13b)) form a closed system. We consider two possible boundary conditions at $x = 0$ of interest:

(i) the surfactant concentration on the adsorbing surface remains constant, (4.12);

(ii) the surfactant concentration on the adsorbing surface is time dependent, (4.13b).

We compare these results with the dimensionless mesoscopic model in section 3.

4.5.1. Constant surfactant concentration on the adsorbing surface. We prescribe a rapidly decaying Gaussian distribution for the initial surfactant distribution so that surfactant is initially localized in a small boundary layer near the surface with negligible concentration in the bulk:

$$B(x,0) = \mathrm{e}^{-(x/\sigma)^2}, \tag{4.34}$$

where σ is taken to be small. We solve (4.5) numerically on the domain $x \in [0,1]$ subject to the boundary conditions (4.9), (4.12), and (4.17) and initial condition (4.34). As for the mesoscopic model, the system evolves from the initial profile to the steady-state solution (4.21) in a smooth manner (Figure 9).

4.5.2. Time-dependent surfactant concentration on the adsorbing surface. In this section we consider the case where the parameters $a_{\mathrm{m}}, b_{\mathrm{m}}$, and d_{m} are of order ϵ^3 so that the boundary condition on the adsorbing surface, to leading order, is time dependent and given by (4.13b). Equation (4.5) can be solved subject to the boundary conditions (4.9), (4.13b), and (4.17), and the initial data

$$B(x,0) = \Gamma_0 \mathrm{e}^{-(x/\sigma)^2}, \tag{4.35}$$

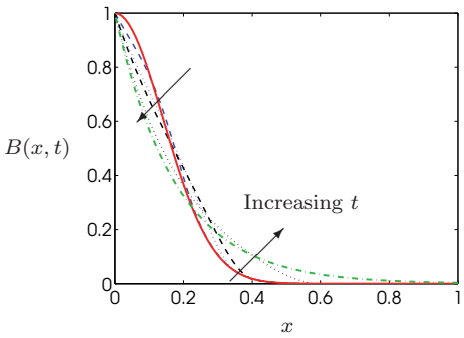

FIG. 9. (a) *Plots of the numerical solution to* (4.5), (4.9), (4.12), *and* (4.17) *at times* $t = 0.0001$ *(blue dashed),* $t = 0.0005$ *(blue dotted),* $t = 0.001$ *(black dashed), and* $t = 0.01$ *(black dotted). The initial condition* (4.34) *is plotted by the red continuous curve for* $\sigma = 0.2$*, and the green dot-dashed curve denotes the steady state solution,* B_0*, given by* (4.21).

via the method of lines on the domain $x \in [0, 1]$. As we would expect, the system evolves from its initial configuration in a qualitatively similar way to that for constant surfactant concentration on the adsorbing boundary in section 4.5.1 but with the surfactant concentration at the adsorbing boundary now evolving with time (Figure 10(a)). Figures 10(b), (c) show the evolution of the numerical solution for $\Gamma(t)$ and $B(0.1, t)$ to the steady-state solution (4.21).

4.5.3. Similarity solution. Clarkson, Mansfield, and Priestley have categorized the symmetry reductions to a general class of third-order nonlinear partial differential equations that includes (4.5) using classical Lie methods [3]. Three reductions to (4.5) were found, namely,

$$B(x,t) = f(\eta), \qquad \eta = x - ct, \tag{4.36a}$$

$$B(x,t) = t^{3m} f(\eta), \qquad \eta = \frac{x}{t^{m+1/3}}, \tag{4.36b}$$

$$B(x,t) = \mathrm{e}^{3mt} f(\eta), \qquad \eta = x\mathrm{e}^{-mt}. \tag{4.36c}$$

In the context of the multilayer problem the physically relevant reduction is (4.36b), with $m = -1/12$ to ensure that mass is conserved. The resulting similarity solution describes the spreading of an initially concentrated distribution of surfactant on an infinite domain $-\infty < x < \infty$. Thus, we replace the boundary conditions on the adsorbing surface, $B = \Gamma$, and (4.9) with the symmetry conditions

$$B_x(0,t) = B_{xx}(0,t) = 0. \tag{4.37}$$

Since one expects the number of bilayers to decay as $x \to \infty$, and given the symmetry of the problem, we make the plausible assumption that $B_x < 0 \ \forall x > 0$. Thus, the reformulated problem to solve using a similarity solution is given on the half-space $x \in [0, \infty)$:

$$B_t = -\left(B_x^2 - BB_{xx}\right)_x, \quad 0 < x < \infty, \tag{4.38a}$$

$$B_x(0,t) = B_{xx}(0,t) = 0, \tag{4.38b}$$

$$B_x^2 - BB_{xx} \to 0 \quad \text{as} \quad x \to \infty. \tag{4.38c}$$

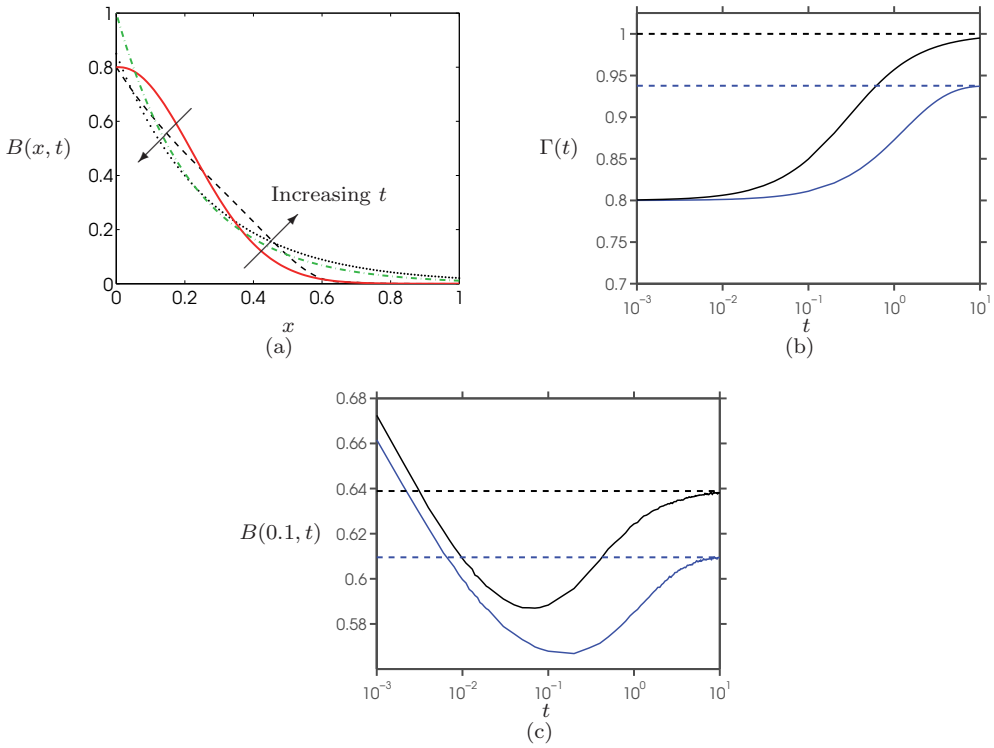

FIG. 10. (a) *Plots of the numerical solution to* (4.5), (4.9), (4.13b), *and* (4.17) *for space step* $\triangle x = 0.01$ *and times* $t = 0.005$ *(black dashed) and* $t = 0.5$ *(black dotted). The initial condition* (4.35) *is denoted by the red continuous curve and the steady-state solution* (4.21) *is denoted by the green dot-dashed curve.* (b) *Plots of the evolution of surface concentration* $\Gamma(t)$ *according to* (4.13b) *(black continuous curve); the steady-state value for* Γ *(black dashed line); the mesoscopic model* (3.2) *(blue-continuous curve) and the steady-state value* (3.8). (c) *Comparison of the numerical solution (black continuous line) against the steady-state solution,* B_0 *(black dashed line), given by* (4.21) *at* $x = 0.1$, *and the corresponding plots for the mesoscopic model (blue curves). Here* $\sigma = 0.3$, $\Gamma_0 = 0.8$, $\alpha_m = 2$, $\beta_m = \delta_m = 0.2$, $a_i = b_i = c_i = d_i = 1$, *and* $K = 100$.

To close the problem we impose net conservation of mass:

$$\int_0^\infty B(x,t)\ \mathrm{d}x = 1, \tag{4.38d}$$

where, without loss of generality, the net concentration of surfactant in $x \in (0,\infty)$ has been scaled to 1.

The corresponding similarity solution is found to have compact support, with

$$B(x,t) = \begin{cases} t^{-1/4} B_0 f(\eta), & 0 < \eta < \eta_c, \\ 0 & \text{otherwise}, \end{cases} \tag{4.39}$$

where $\eta = x t^{-1/4} \Gamma_0^{1/3}$ and the parameters B_0 and η_c are to be determined as part of the solution. Substituting (4.39) into (4.38), integrating (4.38a) with respect to η once, and applying boundary conditions (4.38b) we obtain the initial-value problem

$$f(\eta) f''(\eta) - (f'(\eta))^2 + \frac{1}{4}\eta f = 0, \quad f(0) = 1, \quad f'(0) = 0, \tag{4.40}$$

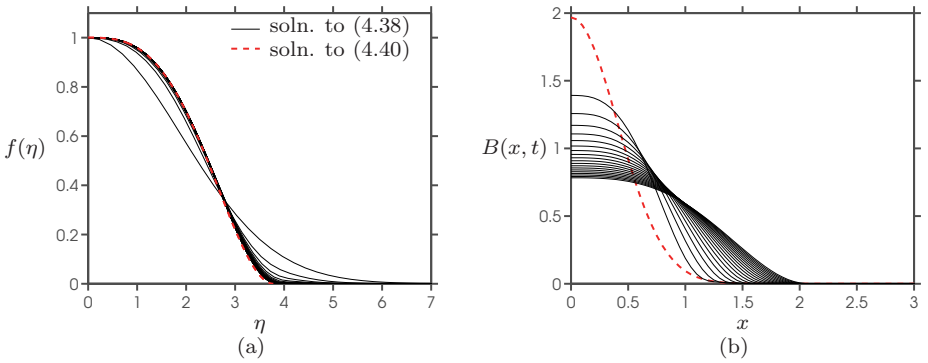

FIG. 11. (a) *Comparison of the numerical solution to* (4.38) *(black curves), with the similarity solution* $f(\eta)$ *given by the numerical solution to* (4.40) *(red dashed curve).* (b) *Numerical solution (black curves) to* (4.38) *subject to the initial condition* (4.43) *(red dashed curve) on the truncated domain* $x \in [0, 10]$ *for* $t \in [0.01, 0.02, \ldots, 0.1]$ *and space step* $\triangle x = 0.1$.

with η_c determined from

$$f(\eta_c) = 0 \tag{4.41}$$

and B_0 determined from the equation for conservation of mass, (4.38),

$$\int_0^{\eta_c} f(\eta)\, \mathrm{d}\eta = B_0^{-4/3}. \tag{4.42}$$

We note that by a suitable change of variable, one can reduce (4.40) to a second-order autonomous ODE, although the result has no known analytical solution. Therefore, we instead compute the solutions to the initial-value problem (4.40) numerically. The numerical values for the parameters $\eta_c \approx 3.784$ and $\Gamma_0 \approx 0.523$ are obtained using (4.41) and (4.42), and the result is displayed in Figure 11(a). We solve (4.38) via the method of lines subject to the initial condition

$$B(x, t_0) = B_0 t_0^{-1/4} \mathrm{e}^{-x^2/\sigma^2}, \quad \sigma = \frac{2t_0^{-1/4}}{\sqrt{\pi}\Gamma_0}, \tag{4.43}$$

and plot $f(\eta) = t^{1/4} B(\eta \Gamma_0^{-1/3} t^{1/4}, t)/B_0$ for different values of t in Figure 11(a), which shows the convergence of the numerical solution to the similarity solution as t increases. The evolution of the concentration, $B(x, t)$, is shown in in Figure 11(b) for reference.

5. Two adsorbing boundaries. Our model system so far has comprised only one adsorbing surface. In this section, we now extend the model by considering a multilayer structure that has formed between two adsorbing surfaces. We now consider a finite dimensionless domain $\mathcal{D} := \{x : x \in [0, 1]\}$ with two monolayers at $x = 0$ and $x = 1$. We define the dimensionless monolayer concentrations at the left- and right-hand boundaries to be $\Gamma_1(t)$ and $\Gamma_2(t)$, respectively. The two adsorbing surfaces may be distinct; for example, one could be an air–liquid interface, while the other could be a solid surface. We suppose that the dimensional saturation concentrations at the left and right boundaries are $\Gamma_{\mathrm{sat},1}$ and $\Gamma_{\mathrm{sat},2}$, respectively, and without loss of generality assume that $\Gamma_{\mathrm{sat},2} \leq \Gamma_{\mathrm{sat},1}$. The derivation of the mesoscopic model for this situation is analogous to that in section 3 and so we omit the details here.

5.1. Governing equations. In section 4 we assumed that given an initial concentration profile that monotonically decreases with distance from the adsorbing boundary, the concentration would remain monotone decreasing for all time and so the $\mathrm{sgn}(B_x)$ term in (4.5) would play no role. However, for the case where there are two adsorbing boundaries, we expect that the concentration should decrease as we move away from each boundary, at least locally to the interfaces. Thus B_x must take different signs in the domain. For simplicity, let us assume that B_x changes sign just once in $0 < x < 1$ and the continuum model may then be described by an implicit-moving-boundary problem.

The analogous continuum limit to the mesoscopic model considered in section 4 for two adsorbing surfaces is given by

$$\frac{\partial B}{\partial t} = \frac{\partial}{\partial x}\left(\mathrm{sgn}(B_x)\left({B_x}^2 - BB_{xx}\right)\right) \quad 0 < x < 1, \quad t > 0, \tag{5.1a}$$

with

$$B(x,t) = \begin{cases} B_1(x,t), & 0 \le x < s(t), \\ B_2(x,t), & s(t) \le x \le 1, \end{cases} \tag{5.1b}$$

where $x = s(t)$ denotes the free boundary where the sign of B_x changes, so that $\mathrm{sgn}(B_x) = \mathrm{sgn}(x - s(t))$. The boundary conditions on the fixed boundaries are

$$(B_{1x})^2 - B_1 B_{1xx} = 0, \qquad B_1 = \Gamma_1(t) \qquad \text{on} \quad x = 0, \tag{5.1c}$$

$$(B_{2x})^2 - B_2 B_{2xx} = 0, \qquad B_2 = \Gamma_2(t) \qquad \text{on} \quad x = 1, \tag{5.1d}$$

and on the free boundary

$$[B]^+_- = [|B_x|]^+_- = \left[\mathrm{sgn}(B_x)\left(B_x^2 - BB_{xx}\right)\right]^+_- = 0 \quad \text{on} \quad x = s(t), \tag{5.1e}$$

where $[\cdot]^+_-$ denotes the jump in the expression across the curve $x = s(t)$. The functions $\Gamma_i(t)$ for $i = 1, 2$ depend on the orders of magnitude of the adsorption rate parameters as described in section 4.2 and are given by

$$\Gamma_i(t) = 1 \qquad \text{if} \quad a^i_{\mathrm{m}}, b^i_{\mathrm{m}}, d^i_{\mathrm{m}} \quad \text{are order 1}, \tag{5.2a}$$

$$\frac{\mathrm{d}\Gamma_i}{\mathrm{d}t} = 2\alpha^i_{\mathrm{m}}(\sigma_i - \Gamma_i)^2\Gamma_i \qquad \text{if} \quad a^i_{\mathrm{m}}, b^i_{\mathrm{m}}, d^i_{\mathrm{m}} \quad \text{are order } \epsilon^3 \tag{5.2b}$$

for $i = 1, 2$, where $\alpha^i_{\mathrm{m}} = a^i_{\mathrm{m}}\epsilon^{-3}$, $\sigma_1 = 1$, and $\sigma_2 = \Gamma_{\mathrm{sat},2}/\Gamma_{\mathrm{sat},1} \le 1$. Equation (5.2a) corresponds to constant surfactant concentration on the adsorbing surface and (5.2b) corresponds to the situation where the adsorbed surfactant concentration evolves with time. The initial conditions are given by

$$B(x,0) = f(x), \quad \Gamma_1(0) = \Gamma_{01}, \quad \text{and} \quad \Gamma_2(0) = \Gamma_{02} \tag{5.3}$$

for some specified function $f(x)$ and constants Γ_{01} and Γ_{02}.

5.2. Steady-state solution. For the case where the two boundaries are identical and $\sigma_2 = 1$, the steady-state solution to (5.1) is given by

$$B_0(x) = \begin{cases} \mathrm{e}^{kx}, & 0 \le x < s, \\ \mathrm{e}^{k(1-x)}, & s \le x \le 1, \end{cases} \tag{5.4}$$

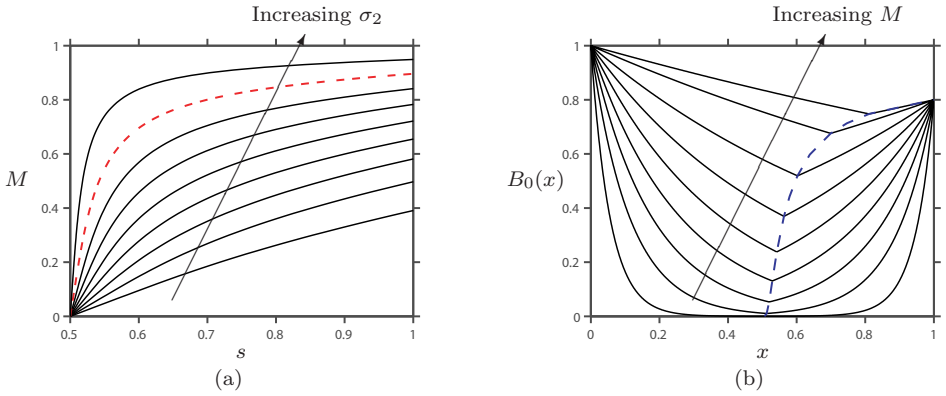

FIG. 12. (a) *Plots of total surfactant concentration, M, against s given by* (5.7) *for* $\sigma_2 \in [0.1, 0.2, \ldots, 0.9]$. *The red curve denotes* $\sigma_2 = 0.8$. (b) *The steady-state solutions,* $B_0(x)$, *given by* (5.6) *are plotted by the black curves for* $M \in [0.1, 0.2, \ldots, 0.8, 0.85]$, *and* $\sigma_2 = 0.8$. *The blue curve denotes* $B_0(s)$.

where $s = 1/2$ and k is given by the implicit equation imposing conservation of mass,

$$M = \frac{2}{k}\left(\mathrm{e}^{k/2} - 1\right). \tag{5.5}$$

When the two boundaries are physically different, $\sigma_2 < 1$, and the steady-state solution to (5.1) is now given by

$$B_0(x) = \begin{cases} {\sigma_2}^{x/(2s-1)}, & 0 \le x < s, \\ {\sigma_2}^{(2s-x)/(2s-1)}, & s \le x \le 1, \end{cases} \tag{5.6}$$

where s is given by the implicit equation

$$M = \frac{(2s-1)}{\log(\sigma_2)}\left(2{\sigma_2}^{s/(2s-1)} - \sigma_2 - 1\right). \tag{5.7}$$

Moreover, since $\sigma_2 < 1$ (5.7) implies that $s > 1/2$ and in the limit $M \to 0$, with σ_2 fixed, we find that $s \to 1/2$. Conversely, in the limit $s \to 1$ we find that the maximum total surfactant concentration is given by

$$M \sim \frac{(\sigma_2 - 1)}{\log(\sigma_2)}. \tag{5.8}$$

The above features of (5.7) are summarized in Figure 12(a), which shows the effect of the relative saturation concentrations, σ_2, and total surfactant concentration, M, on the position of the free boundary, s. In Figure 12(b) we present the steady-state solution, $B_0(x)$, given in (5.6), for different surfactant concentrations, M. The discontinuity in B_0' at $x = s$ appears to vanish as the total surfactant concentration decreases, i.e., $[B_0']^{\pm} \to 0$ as $M \to 0$.

5.3. Time-dependent solutions. To solve (5.1) numerically to determine the time evolution to steady state we first map the problem onto a fixed domain via the

transformation

$$0 < x < s(t): \qquad X = \frac{x}{s(t)}, \qquad B_1(x,t) = U(X,t), \tag{5.9a}$$

$$s(t) < x < 1: \qquad X = \frac{1-x}{1-s(t)}, \qquad B_2(x,t) = V(X,t). \tag{5.9b}$$

Substituting this transformation into (5.1) results in the problem given on $X \in [0,1]$:

$$\frac{\partial U}{\partial t} = -\frac{1}{s(t)^3}\frac{\partial}{\partial X}\left(\left({U_X}^2 - UU_{XX}\right)\right) + \frac{X}{s(t)}\frac{\mathrm{d}s}{\mathrm{d}t}U_X, \tag{5.10a}$$

$$\frac{\partial V}{\partial t} = \frac{1}{(1-s(t))^3}\frac{\partial}{\partial X}\left(\left({V_X}^2 - VV_{XX}\right)\right) - \frac{X}{(1-s(t))}\frac{\mathrm{d}s}{\mathrm{d}t}V_X, \tag{5.10b}$$

$$U = \Gamma_1, \quad V = \Gamma_2, \qquad U_X^2 - UU_{XX} = V_X^2 - VV_{XX} = 0 \qquad \text{on} \quad X = 0, \tag{5.10c}$$

$$U = V, \qquad (s(t)-1)U_X = -s(t)V_X \qquad \text{on} \quad X = 1, \tag{5.10d}$$

$$s(t)^2\left(V_X^2 - VV_{XX}\right) = -(s(t)-1)^2\left(U_X^2 - UU_{XX}\right) \qquad \text{on} \quad X = 1, \tag{5.10e}$$

with initial conditions

$$U(X,0) = f(s(0)X), \qquad V(X,0) = f(1 + (s(0)-1)X). \tag{5.10f}$$

Plots of the numerical solutions to the problem (5.10) subject to the initial conditions

$$f(x) = B_0 + \kappa(x - s_0)^2, \quad s(0) = s_0, \tag{5.11}$$

where κ is a constant, are shown in Figure 13(a). The profile evolves from the initial configuration, instantaneously forming a corner at the moving boundary $x = s(t)$ that persists for all time. The corresponding plot for the evolution of the moving boundary is shown in Figure 13(b) and for large t there is excellent agreement with the steady-state solution. We also observe that, for small t, the free boundary is almost stationary, before the free boundary moves toward the equilibrium in a nonmonotonic fashion as the system undergoes reorganization. In the following section this small-time dynamical behavior of the concentration profile in the region near the free boundary is investigated.

6. Small-time analysis for the formation of "sharp troughs." Thus far we have shown that for both the mesoscopic and macroscopic models, if the initial conditions are nonmonotonic, then we observe the formation and evolution of smooth humps and sharp troughs in the solution, which eventually decay for large time. These nonlinear features in the evolution of the bilayer distribution, for certain initial conditions, suggest that smaller multilayer regions that are separated by regions of lower concentration (sharp troughs) initially form, before eventually combining together to create the final multilayer structure. In this section we probe the initial formation of these sharp trough regions, as exhibited by the mesoscopic model in Figure 5, or the corner at the moving boundary for the macroscopic model shown in Figure 13(a). We may investigate the instantaneous formation of the corner in the macroscopic model by considering the small-t asymptotic expansion of $B(x,t)$ via

$$B \sim B_0 + g_1(\eta)t^{2/3} + g_2(\eta)t^{4/3} + \cdots \quad \text{as} \quad t \to 0, \tag{6.1}$$

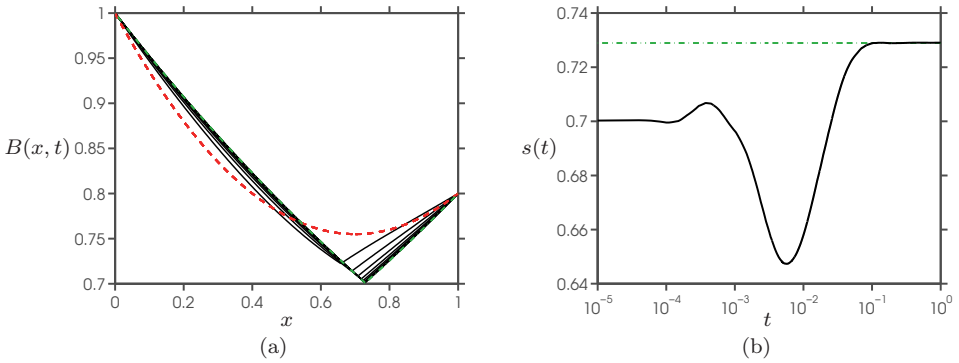

FIG. 13. *Plots of the numerical solution to the macroscopic model for the two-adsorbing-surfaces problem given by* (5.10) *subject to the initial conditions* (5.11) *(red curve). Figure* (a) *shows plots of* $B(x,t)$ *at times* $t \in [0.005, 0.01, \ldots, 0.1]$ *(black curves) and the steady-state solution given by* (5.6)–(5.7) *is denoted by the green curve. The black curve in figure* (b) *compares the evolution of the moving boundary* $s(t)$ *with the steady-state solution for* s*, denoted by the green curve. Here,* $B_0 = 0.755$*,* $\kappa = 0.5$*, and* $s_0 = 0.7$*.*

where $\eta = (x - s_0)t^{-1/3}$ is order one, $s(0) = s_0$, and g_i for $i = 1, 2, \ldots$ are to be determined. Substituting into (5.1a) we obtain an equation for $g_1(\eta)$ at leading order,

$$B_0 \left(\operatorname{sgn}(g_1')g_1''\right)' - \frac{1}{3}\eta g_1' + \frac{2}{3}g_1 = 0. \tag{6.2}$$

We suppose that the initial condition for B is locally quadratic near its minimum at $x = s_0$, so that

$$B(x,t) \sim B_0 + \kappa(x - s_0)^2 + \cdots \quad \text{as} \quad t \to 0 \quad \text{and} \quad x \to s_0. \tag{6.3}$$

Then (6.3) and the boundary conditions (5.1e) to leading order give

$$g_1(\eta) \sim \kappa\eta^2 \qquad \text{as} \quad \eta \to \pm\infty, \tag{6.4}$$

$$[g_1]_-^+ = [|g_1'|]_-^+ = [\operatorname{sgn}(g_1')g_1'']_-^+ = 0 \qquad \text{on} \quad \eta = 0. \tag{6.5}$$

We note that (6.2) is invariant under the transformation $\eta \to -\eta$ and so $g_1(\eta)$ is an odd function. Hence, we may solve the reduced problem on the half-space $\eta > 0$:

$$g_1''' - \frac{1}{3}\eta g_1' + \frac{2}{3}g_1 = 0, \tag{6.6a}$$

$$g_1(\eta) \sim \kappa\eta^2 \qquad \text{as} \quad \eta \to \infty, \tag{6.6b}$$

$$g_1'' = 0 \qquad \text{on} \quad \eta = 0, \tag{6.6c}$$

where we have scaled $\eta \sim B_0^{-1/3}$ and $\kappa \sim B_0^{2/3}$.

Equation (6.6) possesses an explicit solution given by

$$g_1(\eta) = 9\kappa \frac{{}_1F_2(-\frac{2}{3}; \frac{1}{3}, \frac{2}{3}; \frac{\eta^3}{27})}{G\left[-1/3\right]} + 2\kappa\eta \frac{{}_1F_2(-\frac{1}{3}; \frac{2}{3}, \frac{4}{3}; \frac{\eta^3}{27})}{G\left[4/3\right]}, \tag{6.7}$$

where ${}_pF_q(a_1, \ldots, a_p; b_1, \ldots, b_q; z)$ is the generalized hypergeometric function [5] and $G[z]$ denotes the Gamma function [5]. The solution (6.7) is compared with the numerical solution to (5.10) subject to the initial condition (5.11) in Figure 14. As

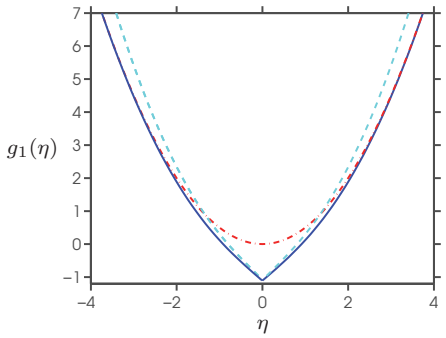

FIG. 14. *Plot of the leading-order similarity solution in the small-t analysis given by* (6.7) *(blue) and the numerical solution to* (5.10) *plotted as* $(B(\eta t^{1/3}+s_0,t)-B_0)t^{-2/3}$ *at* $t=10^{-9}$ *(cyan dot-dashed) subject to the initial condition* (5.11) *(red dot-dashed), for parameters* $B_0=0.755$, $s_0=0.7$, *and* $\kappa=0.5$.

anticipated, the instantaneous appearance of the corner at $\eta=0$ is clear, which is representative of the "sharp troughs," and both curves are observed to match well for small η.

7. Discussion. In this paper we systematically derived mesoscopic and macroscopic models using mass-action kinetics to describe the evolution of surfactant pairs in a multilayer structure consisting of repeating bilayers. The macroscopic description results in a novel nonlinear third-order PDE that provides a continuous description for the concentration of surfactant that exists in the bilayers beneath the adsorbing surface. Of particular interest is the presence of a term that induces a switch in the system characteristics depending on the sign of the concentration gradient. This PDE is coupled to a Langmuir–Hinshelwood-type equation to describe the evolution of the adsorbed surfactant concentration at the surface.

We began by considering the set-up in which a bilayer structure may form beneath a single adsorbing interface. We showed that if the initial distribution of surfactant is monotonically decreasing as we move from the interface, as is typically the case in a surfactant multilayer set-up, then it remains so for all time. However, if the initial conditions are not monotonic, then we observe the formation of "smooth humps" and "sharp troughs" in the evolution of the concentration profile that eventually decay for large time. This is consistent with the physical observation that multilayer structures generally form from distinct lamellar fragments, i.e., smooth humps in the concentration profile, that are separated in space by regions of lower surfactant concentration (sharp troughs).

In steady state, the concentration of surfactant in each bilayer decays exponentially with depth. The resulting steady state was shown to be linearly stable and provides a method for estimating the number of bilayers expected to form given the adsorption properties of the system and the total surfactant concentration, which qualitatively agrees with that observed experimentally [8].

The model was extended to consider the scenario in which there are two adsorbing boundaries. For such a configuration, in steady state the concentration now decreases in an exponential manner as we move away from either boundary, so that the concentration attains a minimum value at some intermediate position that is dictated by the relative adsorption affinity of these interfaces (dimensionless parameter σ_2) and the total mass of surfactant in the system (dimensionless parameter M). With

equal adsorption affinities the minimum occurs at the midpoint between the two interfaces; otherwise, the minimum is located further from the interface with a stronger adsorption affinity. At this minimum, the concentration profile forms a corner that corresponds to a discontinuity in the spatial derivative of the bilayer concentration.

We explored the temporal evolution toward equilibrium of a system with two adsorbing boundaries. In this case, the discontinuity in gradient that is present in the equilibrium distribution was shown to form instantaneously and to evolve with time toward its equilibrium position. To track the motion of this point requires an implicit free-boundary-problem description and appropriate extra conditions to close the problem, and we showed that the early-time formation of this corner can be described by a similarity solution.

The results of this paper have exposed a richness in the kinetic behavior exhibited during the formation and structural reordering of surfactant bilayers. The continuum model derived provides a simplified description that lends itself to ready mathematical analysis that gives insight into the physical behavior observed. The models derived here provide a solid foundation from which generalizations and extensions may be made that should allow for a deeper understanding of the multilayer kinetics that takes place in a range of physical situations.

An interesting generalization to this model would be to examine the impact that the geometry of the adsorbing interface has on the adsorption kinetics. While our one-dimensional model implicitly assumes adsorption at a flat interface, in reality the surface could be curved, introducing the possibilities of crowding. Such a generalization might also be used to provide further understanding of the aggregation process for micelles, in which the geometries of the adsorbing interface are both complex and time varying.

Acknowledgments. The authors gratefully acknowledge helpful discussions with J. Penfold and R. K. Thomas.

REFERENCES

[1] B. Alberts, D. Bray, J. Lewis, M. Raff, K. Roberts, and J. D. Watson, *Molecular Biology of the Cell*, Garland, New York, 1994.

[2] C. Chang and E. I. Franses, *Adsorption dynamics of surfactants at the air/water interface: A critical review of mathematical models, data, and mechanisms*, Colloid Surfaces, 100 (1995), pp. 1–45.

[3] P. A. Clarkson, E. L. Mansfield, and T. J. Priestley, *Symmetries of a class of nonlinear third-order partial differential equations*, Math. Comput. Modelling, 25 (1997), pp. 195–212.

[4] D. Follows, F. Tiberg, R. K. Thomas, and M. Larsson, *Multilayers at the surface of solutions of exogeneous lung surfactant: Direct observation by neutron reflection.*, Biochimica Biophysica Acta, 1768 (2007), pp. 228–235.

[5] I. S. Gradshteyn and I. M. Ryzhik, *Tables of Integrals, Series, and Products*, Academic Press, New York, 2007.

[6] B. A. Hills, *An alternative view of the role(s) of surfactant and the alveolar model*, J. Appl. Physiology, 87 (1999), pp. 1567–1583.

[7] T. Kawai, Y. Yamada, and T. Kondo, *Adsorbed monolayers of mixed surfactant solutions of sodium dodecylsulfate and cetylpyridinium chloride studied by infrared external reflection spectroscopy*, J. Phys. Chem., 112 (2008), pp. 2040–2044.

[8] J. Penfold, *private communication*, 2012.

[9] J. Penfold, R. K. Thomas, C. C. Dong, I. Tucker, K. Metcalfe, S. Golding, and I. Grillo, *Equilibrium surface adsorption behaviour in complex anionic/nonionic surfactant mixtures.*, Langmuir, 23 (2007), pp. 10140–10149.

[10] J. T. Petkov, I. M. Tucker, J. Penfold, R. K. Thomas, D. N. Petsev, C. C. Dong, S. Golding, and I. Grillo, *The impact of multivalent conterions Al^{3+}, on the surface*

adsorption and self-assembly of the anionic surfactant alkyloxyethylene sulfate and anionic/nonionic surfactant mixtures, Langmuir, 26 (2010), pp. 16699–16709.

[11] M. Rosen, *Phenomena in Mixed Surfactant Systems*, ACS Symposium Ser. 311, American Chemical Society, Washington, DC, 1988.

[12] J. F. Scamehorn, *Mixed Surfactant Systems*, Marcel Dekker, New York, 1992.

[13] T. P. Stevens, M. Blannow, E. H. Myers, and R. Soll, *Early surfactant administration with brief ventilation vs. selective surfactant and continued mechanical ventilation for preterm infants with or at risk for respiratory distress syndrome*, Cochrane Database Systematic Rev., 4 (2007).

[14] I. Tucker, J. Penfold, R. K. Thomas, C. C. Dong, S. Golding, C. Gibson, and I. Grillo, *The adsorption and self-assembly of mixtures of alkylbenzene sulfonate isomers and the role of divalent electrolyte*, Langmuir, 27 (2011), pp. 6674–6682.